RESEARCH ARTICLE

WILEY

Multiparametric and multilevel characterization of morphological alterations in patients with transient ischemic attack

Yating Lv[1,2,3,4] | Wei Wei[1,2,3,4] | Xiujie Han[4] | Yulin Song[4] | Yu Han[5] | Chengshu Zhou[4] | Dan Zhou[4] | Fuding Zhang[4] | Xiaoyan Wu[6] | Jinling Liu[7] | Lijuan Zhao[4] | Cairong Zhang[4] | Ningkai Wang[8,9] | Jinhui Wang[8,9]

[1]Center for Cognition and Brain Disorders, The Affiliated Hospital of Hangzhou Normal University, Zhejiang, Hangzhou, China

[2]Institute of Psychological Science, Hangzhou Normal University, Zhejiang, Hangzhou, China

[3]Zhejiang Key Laboratory for Research in Assessment of Cognitive Impairments, Zhejiang, Hangzhou, China

[4]Department of Neurology, Anshan Changda Hospital, Anshan, Liaoning, China

[5]Department of Neurology, The First Affiliated Hospital, Dalian Medical University, Dalian, Liaoning, China

[6]Department of Image, Anshan Changda Hospital, Anshan, Liaoning, China

[7]Department of Ultrasonics, Anshan Changda Hospital, Anshan, Liaoning, China

[8]Institute for Brain Research and Rehabilitation, Guangdong Key Laboratory of Mental Health and Cognitive Science, Center for Studies of Psychological Application, South China Normal University, Guangzhou, China

[9]Key Laboratory of Brain, Cognition and Education Sciences (South China Normal University), Ministry of Education, Guangzhou, China

Correspondence
Jinhui Wang, Institute for Brain Research and Rehabilitation, South China Normal University, Guangzhou 510631, China.
Email: jinhui.wang.1982@m.scnu.edu.cn

Abstract

Transient ischemic attack (TIA), an important risk factor for stroke, is associated with widespread disruptions of functional brain architecture. However, TIA-related structural alterations are not well established. By analyzing structural MRI data from 50 TIA patients versus 40 healthy controls (HCs), here we systematically investigated TIA-related morphological alterations in multiple cortical surface-based indices (cortical thickness [CT], fractal dimension [FD], gyrification index [GI], and sulcal depth [SD]) at multiple levels (local topography, interregional connectivity and whole-brain network topology). For the observed alterations, their associations with clinical risk factors and abilities as diagnostic and prognostic biomarkers were further examined. We found that compared with the HCs, the TIA patients showed widespread morphological alterations and the alterations depended on choices of morphological index and analytical level. Specifically, the patients exhibited: (a) regional CT decreases in the transverse temporal gyrus and lateral sulcus; (b) impaired FD- and GI-based connectivity mainly involving visual, somatomotor and ventral attention networks and interhemispheric connections; and (c) altered GI-based whole-brain network efficiency and decreased FD-based nodal centrality in the middle frontal gyrus. Moreover, the impaired morphological connectivity showed high sensitivities and specificities for distinguishing the patients from HCs. Altogether, these findings demonstrate the emergence of morphological index-dependent and analytical level-specific alterations in TIA, which provide novel insights into neurobiological mechanisms underlying TIA and may serve as potential biomarkers to help diagnosis of the disease. Meanwhile, our findings highlight the necessity of using multiparametric and multilevel approaches for a complete mapping of cerebral morphology in health and disease.

KEYWORDS

brain network, cortical surface, morphology, structural MRI, transient ischemic attack

1 | INTRODUCTION

According to the WHO guidelines, transient ischemic attack (TIA) is defined as a sudden onset of neurological symptoms due to vascular etiology that resolve within 24 hr (Albers et al., 2002; Easton et al., 2009). Although the episodes of symptoms are transient, persistent cognitive impairments occur to patients with TIA in multiple domains (Bakker et al., 2003; Sachdev et al., 2004; Su et al., 2018). Moreover, patients with TIA have a high risk of suffering from stroke (Giles & Rothwell, 2007). Therefore, characterizing structural and functional brain alterations in TIA is of great significance not only for understanding neurobiological substrate of TIA but also for early diagnosis and intervention of stroke.

Advanced multimodal MRI techniques provide powerful tools to study structural and functional alterations in various brain disorders in vivo. With respect to TIA, existing studies mainly employ resting-state functional MRI to explore brain alterations in patients. It has been shown that TIA is associated with disrupted functional brain architecture at multiple levels, including disturbances in local neural activity (Guo et al., 2014; Lv, Li, et al., 2019), breakdown of interregional functional connectivity (Li et al., 2013; Zhu et al., 2019), and disruption of large-scale network topology (Lv, Han, et al., 2019). Regarding TIA-related structural alterations, there is only one study so far that examined gray matter volume in patients via a voxel-based morphometry analysis of structural MRI (sMRI) data (Li et al., 2015). However, volumetric measures derived from the voxel-based morphometry approaches are thought to reflect a composite of multiple morphological indices (Hutton, Draganski, Ashburner, & Weiskopf, 2009; Voets et al., 2008), and thus may overlook specific morphological alterations in TIA.

The human cerebral cortex is a highly complex, folded structure, whose morphological architecture can be captured from different aspects through various morphological indices, such as cortical thickness (CT), fractal dimension (FD), gyrification index (GI), and sulcal depth (SD). Moreover, previous studies have shown that different morphological indices are associated with distinct genetic influences (Panizzon et al., 2009; Strike et al., 2019; Winkler et al., 2010) and exhibit differential developmental and aging trajectories (Hogstrom, Westlye, Walhovd, & Fjell, 2013; Raznahan et al., 2011; Wierenga, Langen, Oranje, & Durston, 2014). These findings suggest that different morphological indices are largely independent of each other. Therefore, it is important to utilize multiple indices to provide a more precise and specific characterization of morphological alterations in TIA. Further, beyond local morphological architecture, numerous studies have shown that areas within the same neuroanatomical circuits show morphological covariance across participants (Andrews, Halpern, & Purves, 1997; Lerch et al., 2006), forming whole-brain morphological covariance networks (Bassett et al., 2008; He, Chen, & Evans, 2007). In particular, as recent methodology progresses, such morphological covariance networks can be mapped at the individual level (Kong et al., 2015; Tijms, Series, Willshaw, & Lawrie, 2012; Wang, Jin, Zhang, & Wang, 2016), which are able to account for interindividual variability in cognition and behavior and act as diagnostic

biomarkers for brain diseases (Chen et al., 2017; Li & Kong, 2017; Seidlitz et al., 2018). With respect to TIA, however, it remains largely unknown whether and how interregional morphological connectivity and whole-brain morphological network organization are disrupted.

In this study, we aim to provide a comprehensive mapping of morphological alterations in patients with TIA. To this end, four cortical surface mesh-based indices (CT, FD, GI, and SD) were employed to investigate morphological alterations in 50 patients with TIA versus 40 healthy controls (HCs) at the level of: (a) local topography by univariate analysis of regional mean in each of 148 regions of interest (ROIs); (b) interregional morphological connectivity via bivariate analysis of morphological covariance between each pair of the 148 ROIs; and (c) whole-brain morphological network organization through multivariate analysis of large-scale morphological covariance patterns among the 148 ROIs. For the observed morphological alterations, we further examined their associations with risk factors for TIA and their potential as biomarkers to distinguish the patients from controls and predict ischemic attacks of the patients during 1-year follow-up.

2 | MATERIALS AND METHODS

2.1 | Participants

Following the WHO guidelines, we recruited 51 patients with TIA who had transient (i.e., less than 24 hr) neurologic symptoms due to a possible vascular etiology as evaluated by experienced clinical neurologists. The patients were from the Department of Neurology, Anshan Changda Hospital from April 2015 to June 2016. Patients with hemorrhage, leukoaraiosis, epilepsy, migraine or a history of psychiatric disease were excluded from this study. For each patient, we recorded the following information: (a) history of TIA and stroke; (b) risk factors including hypertension, diabetes mellitus, coronary artery disease, current smoking, and drinking; (c) medications used before the MR scanning; (d) in-hospital evaluation of arterial stenosis (carotid duplex ultrasound and MR angiography), atrial fibrillation (electrocardiogram) and brain infarcts (diffusion-weighted imaging and T2-FLAIR); and (e) 1-year telephone follow-up of stroke and/or TIA. Based on the methods described previously, an score which considered age, blood pressure, clinical features, duration of symptoms, and history of diabetes (ABCD2) was obtained for each patient to evaluate the risk for subsequent stroke (Johnston et al., 2007). One patient was excluded due to loss of the structural image, leaving 50 TIA patients (39 males; age = 57.340 ± 9.768 years) in the final analyses. Out of the 50 patients, 4 (8%) experienced a history of stroke, 25 (50%) had a history of TIA, 6 (12%) had white matter hyperintensity in diffusion-weighted images, and 9 (18%) had intracranial large-vessel stenosis or carotid artery stenosis. The transient symptoms of the patients included difficulties moving left (21 patients, 43.8%) or right (18 patients, 37.5%) side of the body, numbness in the left limb (3 patients, 6.3%), sudden loss of vision (6 patients, 12.5%), mouth droop (1 patient, 2.1%) and speaking difficulty (21 patients, 43.8%). In addition, 40 age- and sex-matched HCs (29 males;

age = 55.300 ± 7.936 years) were recruited from the local community via advertisements. The HCs had no physical diseases or history of psychiatric or neurologic diseases. This study was approved by the Ethics Committee of the Center for Cognition and Brain Disorders, Hangzhou Normal University. Written informed consent was obtained from each participant.

2.2 | Clinical procedure

All participants completed a series of physiological and biochemical tests within 24 hr before the MR scanning, including blood systolic pressure, blood diastolic pressure, blood sugar level, cholesterol, triglycerides, high-density lipoprotein cholesterol and low-density lipoprotein cholesterol. In addition, all participants underwent the mini-mental state examination (MMSE) to evaluate global cognition (Schultz-Larsen, Lomholt, & Kreiner, 2007).

2.3 | sMRI data acquisition

All MRI data for both the TIA patients and HCs were acquired using a 3.0 T scanner (MR750, GE Medical Systems, Waukesha, WI) at Anshan Changda Hospital. To minimize the effects of scanner states and body rhythms of participants as much as possible, the MR scanning was performed at around 3:00 p.m.–5:00 p.m. for most participants (46 out of the 51 patients and 35 out of the 40 HCs). The MR scanning was performed from 6 hr to 16 days (2.673 ± 2.978 days) after the last TIA for all patients. sMRI data were acquired using a 3D-MPRAGE sequence: 176 sagittal slices; repetition time = 8,100 ms; echo time = 3.1 ms; matrix = 256×256; field of view = 256×256 mm^2; and thickness/gap = 1.0/0 mm. This session lasted for about 5 min.

2.4 | sMRI data preprocessing

The sMRI data were processed with Computational Anatomy Toolbox (CAT12, http://www.neuro.uni-jena.de/cat) based on Statistical Parametric Mapping software (SPM12, http://www.fil.ion.ucl.ac.uk/spm/softwarespm12). CAT12 offers a volume-based approach for estimating regional CT without extensive reconstruction of cortical surface and has been proved to be a fast and reliable alternative to FreeSurfer (Righart et al., 2017; Seiger, Ganger, Kranz, Hahn, & Lanzenberger, 2018).

Briefly, individual structural images were first segmented into gray matter, white matter and cerebrospinal fluid. Then, estimation of CT and reconstruction of central surface were performed based on a projection-based thickness method (Dahnke, Yotter, & Gaser, 2013). Specifically, this method estimates white matter distance and projects the local maxima to other gray matter voxels using a neighbor relationship described by the white matter distance (Dahnke et al., 2013). The projection-based thickness method could handle the partial volume

information, sulcal blurring, and sulcal asymmetries. The reconstruction of the central surface uses topology correction (Yotter, Dahnke, Thompson, & Gaser, 2011) and spherical mapping (Yotter, Thompson, & Gaser, 2011). In addition, CAT12 allows estimation of other morphological indices of FD, GI, and SD, which were also calculated for each participant with default parameter settings. The calculation of CT, FD, GI, and SD was performed in subject native surface space. Finally, the resultant morphological maps were resampled into the common fsaverage template and smoothed using a Gaussian kernel (15-mm full width at half maximum for CT and 25-mm full width at half maximum for the others). The usage of larger filter sizes for the FD, GI, and SD maps is due to the underlying nature of these folding measures that reflect contributions from both sulci and gyri, and thus the filter size should exceed the distance between a gyral crown and a sulcal fundus.

2.5 | Construction of individual morphological brain networks

In this study, we constructed four large-scale morphological brain networks for each participant based on their four vertexwise surface maps of CT, FD, GI, and SD. A brain network is comprised of a collection of nodes linked by edges, wherein nodes represent brain regions and edges represent interregional connectivity. The method used to construct single-subject morphological brain networks has been shown to have high both short-term and long-term test–retest reliability in previous studies (Kong et al., 2015; Wang et al., 2016).

2.5.1 | Node definition

To define network nodes, we utilized a widely used surface atlas (Destrieux, Fischl, Dale, & Halgren, 2010) to parcel the cerebral cortical surface into 148 ROIs, with each ROI representing a node.

2.5.2 | Edge definition

To estimate network edges, we calculated morphological connectivity between any pair of ROIs using a method similar to our previous study (Wang et al., 2016). First, for each morphological index we extracted all values within each ROI in the surface-based space, which were used to estimate regional probability density functions using a normal kernel function (MATLAB function, ksdensity). After converting the resultant probability density functions to probability distribution functions (PDFs), we calculated the Jensen–Shannon divergence (JSD) between any pair of PDFs, a variation of the Kullback–Leibler divergence (KLD). Formally, for two PDFs P and Q, the KLD and JSD are calculated as:

$$KLD(P||Q) = \sum_{i=1}^{n} P(i)\log\frac{P(i)}{Q(i)} \text{ and } JSD(P||Q) = \frac{1}{2}KLD(P||M) + \frac{1}{2}KLD(Q||M),$$

where $M = \frac{1}{2}(P + Q)$, and n is the number of sample points (256 in the current study). Finally, the morphological connectivity between two regions was defined as the square root of the JSD, followed by a subtraction from 1. This resulted in four 148×148 morphological connectivity matrices for each participant.

2.5.3 | Threshold selection

For the morphological connectivity matrices derived above, a sparsity-based thresholding procedure was employed to convert each of them to a set of binary networks. Sparsity is defined as the ratio of the number of actual edges divided by the maximum possible number of edges in a network. Thus, the sparsity-based thresholding procedure ensures the same number of edges for the resultant networks across participants at a fixed sparsity. Due to the lack of a conclusive method to determine a single sparsity, we repeatedly thresholded each morphological connectivity matrix over a consecutive sparsity range of [0.04 0.4] with an interval = 0.02. This sparsity range guarantees that the resultant networks have sparse properties (Achard, Salvador, Whitcher, Suckling, & Bullmore, 2006; Wang et al., 2009) and are estimable for the small-world attributes (Watts & Strogatz, 1998).

2.6 | Network analysis

For each morphological brain network derived above (90 participants × 4 morphological indices × 18 sparsity levels), we calculated four efficiency measures (local efficiency, global efficiency, normalized local efficiency, and normalized global efficiency) to characterize their global organization and five nodal centrality measures (degree, efficiency, betweenness, eigenvector, and page-rank) to capture local roles of each node within them.

2.6.1 | Network efficiency measures

Global efficiency reflects the ability of parallel information processing of a network, while local efficiency measures the fault tolerance of a network (Latora & Marchiori, 2001). To determine whether morphological brain networks were topologically organized into small-world organization, global efficiency and local efficiency were normalized by the corresponding mean derived from 100 random networks that preserved the same degree distributions as the real brain networks (Maslov & Sneppen, 2002; Milo et al., 2002). Typically, a network is said to be small world if it has a normalized local efficiency larger than 1 and a normalized global efficiency approximately equal to 1 (Wang et al., 2009; Watts & Strogatz, 1998).

2.6.2 | Nodal centrality measures

Nodal degree quantifies the overall connectivity of a node with other nodes in a network. Nodal efficiency reflects the ability of a node to propagate information with other nodes in a network (Achard & Bullmore, 2007). Nodal betweenness captures the influence of a node over information flow among other nodes in a network (Freeman, 1977). Nodal eigenvector centrality is able to quantify the importance of a node by taking into account not only the degree but also the eigenvector centrality of its neighbors in a network (Bonacich, 1972). As a variant of eigenvector centrality, nodal page-rank centrality introduces a small probability of random damping (i.e., damping factor) to handle walking traps in a network (Boldi, Santini, & Vigna, 2009). For each type of morphological brain network of each group, a node was identified as a hub if its average across participants was at least 1 SD greater than the average across all participants and nodes in at least one of the five nodal centrality measures (Tian, Wang, Yan, & He, 2011).

Notably, given that each network measure was a curve or function of sparsity, we calculated the area under the curve (i.e., the integral over sparsity range) for each network measure of each participant to provide a threshold-independent summary scalar for the hub identification and subsequent statistical analyses.

2.7 | STATISTICAL ANALYSIS

2.7.1 | Between-group differences in local topography (intraregional mean)

A nonparametric permutation test was used to inter between-group differences in each morphological index in a ROI-wise manner. Briefly, for each morphological index of each ROI, we initially calculated the between-group difference of the mean values. An empirical distribution of the difference was then obtained by randomly reallocating all of the values into two groups and recomputing the mean differences between the two randomized groups (10,000 permutations). The 95th percentile point of the empirical distribution was used as a critical value in a one-tailed test of whether the observed group difference could occur by chance. For each morphological index, a Bonferroni method was employed to correct for multiple comparisons across the 148 ROIs. Prior to the permutation tests, the general linear model was used to remove effects of age and sex from the mean of each morphological index within each ROI. In detail, the mean of each morphological index within each ROI was treated as a dependent variable, and age and sex were treated as independent variables in the general linear model. The residuals from the model were used for the permutation tests. For significant between-group differences, the effect size (i.e., Cohen's d) was calculated as the difference between the means of two groups divided by the pooled SD (Cohen, 1969; Cohen, 1987) based on age- and sex-adjusted data.

2.7.2 | Between-group differences in interregional morphological connectivity

We employed a network-based-statistic approach (Zalesky, Fornito, & Bullmore, 2010) to localize the regional pairs showing altered

morphological connectivity in TIA. Briefly, a t statistic matrix was first derived by performing two-sample t test for each connection between the two groups. Analogous to comparisons of local topography, the general linear model was used to remove effect of age and sex from morphological connectivity between each pair of regions before the two-sample t tests. An initial significance threshold (i.e., $p < .001$) was then applied to screen suprathreshold links, among which all connected components and their associated sizes (i.e., the number of edges) were determined. Subsequently, a null distribution of component size was empirically derived for each connected component using a nonparametric permutation approach (10,000 permutations). Finally, the corrected p-value for a connected component with a size of M was determined by calculating the proportion of the 10,000 permutations for which the maximal component size was larger than M.

2.7.3 | Between-group differences in whole-brain morphological network measures

Between-group differences in global and nodal network measures were also inferred using nonparametric permutation tests. For each type of morphological brain networks, the Bonferroni method was used to separately correct for multiple comparisons across 4 global measures and across 148 nodes for each nodal centrality measure. Again, effects of age and sex were removed via the general linear model, and the Cohen's d was calculated for any measures showing significant between-group differences.

2.7.4 | Relationship between morphological alterations and clinical variables in TIA

Kolmogorov–Smirnov tests were first employed to test the normality of metrics showing TIA-related alterations and clinical variables (ABCD2 score, blood systolic pressure, blood diastolic pressure, blood sugar level, cholesterol, triglycerides, high-density lipoprotein cholesterol, and low-density lipoprotein cholesterol) of the patients. For regions, edges and network measures showing TIA-related morphological alterations, Pearson or Spearman partial correlation analyses were then conducted to assess their associations with clinical variables with age and sex as covariates of noninterest.

2.7.5 | Differentiating the TIA patients from HCs

For regions, edges and network measures showing TIA-related morphological alterations, we plotted the receiver operating characteristic (ROC) curves to test whether they might serve as potential biomarkers for differentiating the TIA patients from controls. Specifically, for each metric showing TIA-related alterations, many different thresholds were used to classify each participant into either patient or control group. For each threshold, the fraction of correctly identified patients (i.e., sensitivity or true positive rate) and the fraction of correctly

identified controls (i.e., specificity or true negative rate) were calculated. Finally, a cut-off point that simultaneously optimized the sensitivity and specificity was determined and the classification accuracy at the cut-off point was calculated as the fraction of correctly identified participants (both controls and patients) in the total samples. These procedures were performed using public codes (https://github.com/dnafinder/roc).

In addition to plotting the ROC curves based on one-dimensional features, we utilized the support vector machine (SVM) method which can handle multivariate features. Specifically, we separately trained a linear SVM classifier based on features derived from different combinations of morphological index and analytical level as well as all features of local topography, interregional connectivity and whole-brain network topology derived from CT, FD, GI, and SD. The accuracies of the classifiers were evaluated via 10-fold cross-validation.

2.7.6 | Exploratory analysis of follow-up ischemic attacks in the TIA patients

For regions, edges and network measures showing TIA-related morphological alterations, we further compared their differences between the patients suffering from ischemic attacks in 1 year after the MR scanning and those without follow-up ischemic attacks (permutation tests). For significant between-group differences (corrected by the Bonferroni method across all metrics showing TIA-related morphological alterations), the ROC analyses were further conducted to test their capabilities for predicting follow-up ischemic attacks in TIA.

2.8 | Validation analysis

2.8.1 | Effects of TIA history

In this study, some patients had a history of TIA before the last ischemic attack. To evaluate the effect of TIA history on the observed TIA-related morphological alterations, we compared their differences between patients with more than an ischemic attack (25) and patients who suffered first-time ischemic attack (25) via nonparametric permutation tests (10,000 times).

2.8.2 | Effects of symptom durations

To test whether the observed TIA-related morphological alterations were dependent on symptom durations of the patients, we calculated Spearman correlations between the morphological alterations and symptom durations of the last TIA attack for the patients.

2.8.3 | Effects of brain lesions

Six patients were found to have white matter hyperintensities in our study (Supplementary Figure 1). To rule out the effects of lesions on

our findings, we reanalyzed between-group differences after excluding the six patients with brain lesions.

3 | RESULTS

3.1 | Demographic and clinical characteristics of participants

Demographic and clinical information of all participants are summarized in Table 1. There were no significant differences in age ($p = .288$), sex ($p = .546$), or MMSE scores ($p = .170$) between the TIA patients and HCs. Compared with the HCs, the TIA patients exhibited significantly higher blood systolic pressure ($p < .001$), diastolic pressure ($p = .003$), blood sugar level ($p < .001$), total cholesterol ($p = .043$) and low-density lipoprotein cholesterol ($p = .005$).

3.2 | TIA-related alterations in local morphological topography

Compared with the HCs, the TIA patients exhibited significant alterations in regional CT ($p < .05$, Bonferroni corrected), as characterized by decreases in the left anterior transverse temporal gyrus ($p = .0001$, Cohen's $d = 0.914$), the left posterior ramus of the lateral sulcus ($p = .0001$, Cohen's $d = 0.829$) and the right vertical ramus of the anterior segment of the lateral sulcus ($p = .0001$, Cohen's $d = 1.014$) (Figure 1). No regions were observed to show TIA-related alterations in regional FD, GI or SD ($p > .05$, Bonferroni corrected).

Of note, no significant between-group differences were found when the multiple comparison correction was performed across all tests (592 = 4 morphological indices × 148 regions) ($p > .05$, Bonferroni corrected).

TABLE 1 Demographics and clinical characteristics of all participants

	TIA ($n = 50$)	HCs ($n = 40$)	p-Value
Age (years)	57.340 ± 9.768	55.300 ± 7.936	.288[a]
Sex, No. (M/F)	39/11	29/11	.546[b]
MMSE[c]	29.240 ± 2.560	28.579 ± 1.671	.170[a]
Blood systolic pressure (mmHg)[d]	145.120 ± 20.655	127.188 ± 19.730	<.001[a]
Blood diastolic pressure (mmHg)[d]	86.800 ± 10.388	79.531 ± 10.680	.003[a]
Blood sugar level (mmol/L)[e]	6.263 ± 2.077	5.108 ± 0.748	.001[a]
Total cholesterol (mmol/L)[e]	5.232 ± 1.114	4.741 ± 1.023	.043[a]
Triglycerides (mmol/L)[e]	1.613 ± 0.953	1.875 ± 1.341	.298[a]
HDL-C (mmol/L)[e]	1.107 ± 0.234	1.053 ± 0.294	.350[a]
LDL-C (mmol/L)[e]	3.306 ± 0.956	2.697 ± 0.917	.005[a]
ABCD2 scores, median (min–max)	4 (2–6)		
Smoking, no. (%)	32 (64%)	19 (47.5%)	.116[b]
Drinking, No. (%)	20 (40%)	20 (50%)	.343[b]
Hypertension, No. (%)	24 (48%)	7 (17.5%)	.002[b]
Diabetes, No. (%)	8 (16%)	0 (0%)	.008[b]
Coronary artery disease, No. (%)	2 (4%)	0 (0%)	.201[b]
Atrial fibrillation, No. (%)	1 (2%)		
Medication			
Antiplatelets, No. (%)	50 (100%)		
Statins, No. (%)	2 (4%)		
White matter hyperintensity, No. (%)	6 (12%)		
Vessel stenosis, No. (%)	9 (18%)		
TIA/stroke attack in 1-year follow-up, No. (%)[f]	12 (24%)		

Note: Data are presented as mean ± *SD* unless stated otherwise.
Abbreviations: F, female; HCs, healthy controls; HDL-C, high-density lipoprotein cholesterol; LDL-C, low-density lipoprotein cholesterol; M, male; MMSE, mini-mental state examination; TIA, transient ischemic attack.
[a]p-Values were obtained using two-sample two-sided *t* tests.
[b]p-Values were obtained using Pearson chi-square tests.
[c]Data were missing for two controls.
[d]Data were missing for eight controls.
[e]Data were missing for six controls.
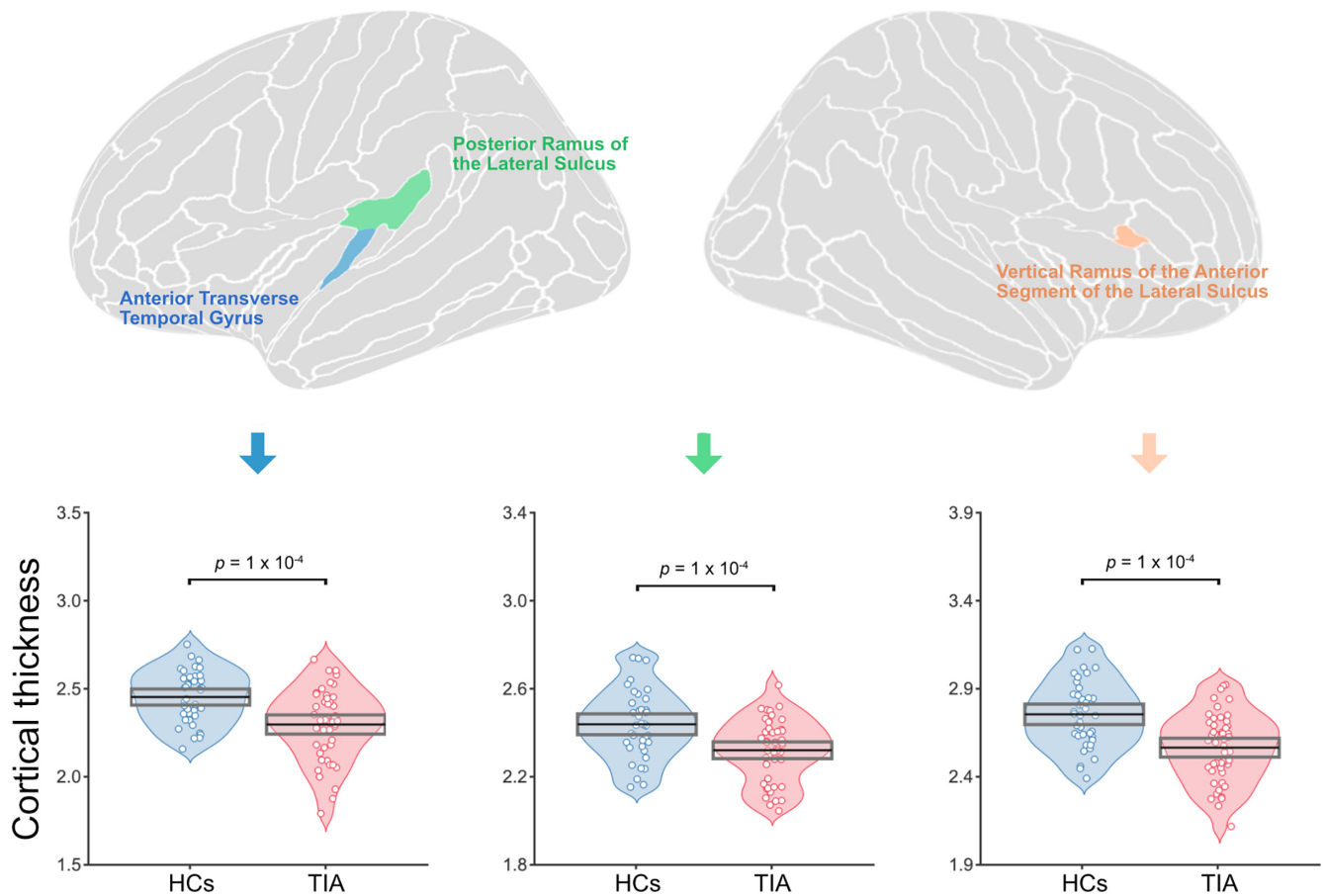[f]Data were missing for four patients.

FIGURE 1 Decreased regional cortical thickness in transient ischemic attack (TIA). Compared with the healthy controls (HCs), the TIA patients exhibited significant decreases in regional cortical thickness (CT) in the left anterior transverse temporal gyrus, the left posterior ramus of the lateral sulcus and the right vertical ramus of the anterior segment of the lateral sulcus ($p < .05$, Bonferroni corrected)

3.3 | TIA-related alterations in interregional morphological connectivity

Two connected components were identified to exhibit decreased morphological connectivity in the TIA patients in comparison with the HCs: one was derived from the FD-based morphological networks that included 29 nodes and 32 edges ($p = .009$, corrected), and the other was derived from the GI-based morphological networks that included 17 nodes and 18 edges ($p = .046$, corrected) (Figure 2). According to the functional connectivity networks proposed by Yeo et al. (2011), 18 out of the 29 nodes (62.1%) included in the FD-based component were involved in visual, somatomotor, ventral attention and default mode networks, while 14 out of the 17 nodes (82.4%) included in GI-based component were involved in visual, somatomotor, and ventral attention networks (Figure 2). For edges included in the two components, the majority was interhemispheric connections (FD-based component: 20/32, 62.5%; GI-based component: 10/18, 52.6%). No components were found to show TIA-related morphological connectivity alterations for neither CT- nor SD-based morphological networks.

3.4 | TIA-related alterations in whole-brain morphological network measures

3.4.1 | Global network efficiency

First, all types of morphological brain networks exhibited highly efficient small-world organization in both groups, as characterized by larger-than-1 normalized local efficiency and approximately-equal-to-1 normalized global efficiency (Figure 3). Nevertheless, between-group comparisons revealed significant alterations in quantitative values of network efficiency in the patients ($p < .05$, Bonferroni corrected). Specifically, compared with the HCs, the TIA patients exhibited significant increases in local efficiency ($p = .007$, Cohen's $d = 0.590$), global efficiency ($p = .006$, Cohen's $d = 0.568$), and normalized global efficiency ($p = .009$, Cohen's $d = 0.567$), and decreases in normalized local efficiency ($p = .007$, Cohen's $d = 0.500$) for GI-based morphological brain networks (Figure 4). No TIA-related network efficiency alterations were observed for CT-, FD-, or SD-based morphological brain networks ($p > .05$, Bonferroni corrected).
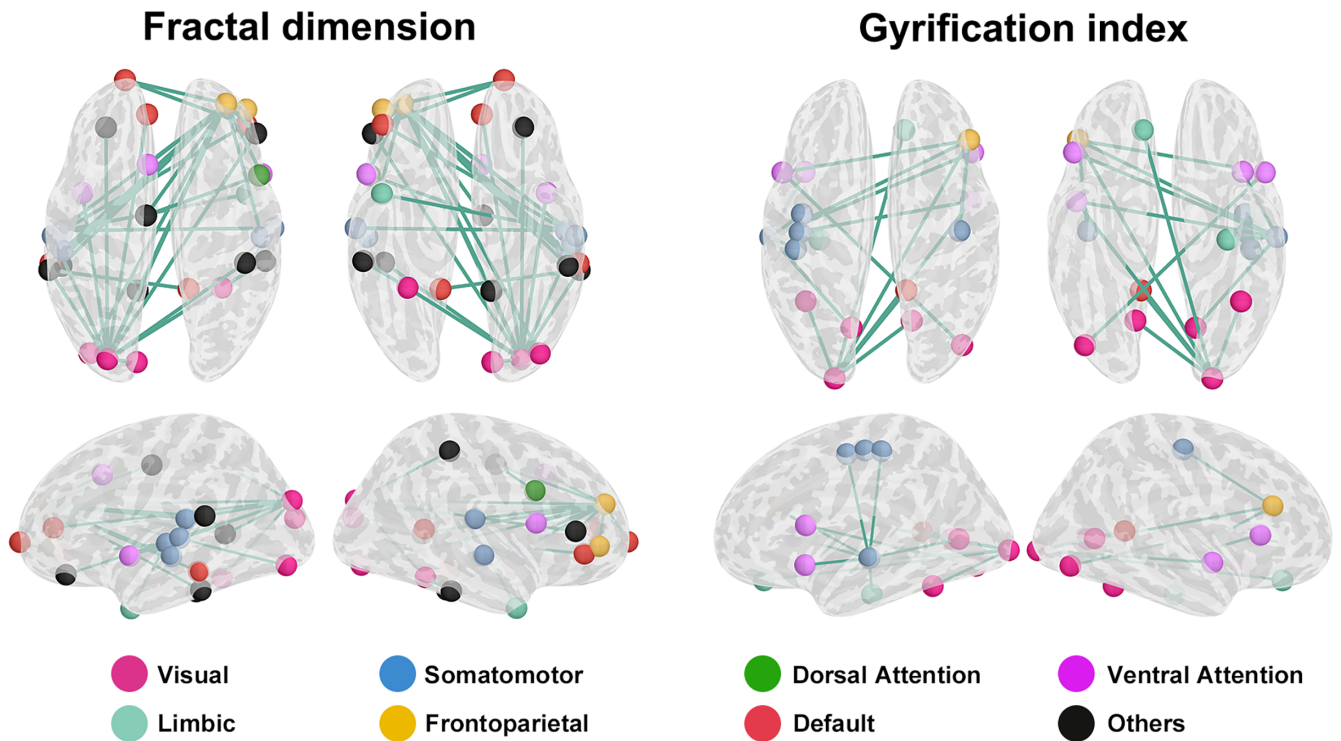
FIGURE 2 Impaired interregional morphological connectivity in transient ischemic attack (TIA). Compared with the healthy controls (HCs), two connected components were identified to exhibit decreases in fractal dimension (FD)-based (a) and gyrification index (GI)-based (b) morphological connectivity in the TIA patients. The components were mainly involved in regions of the visual, somatomotor, and ventral attention networks, and were mainly composed of interhemispheric connections
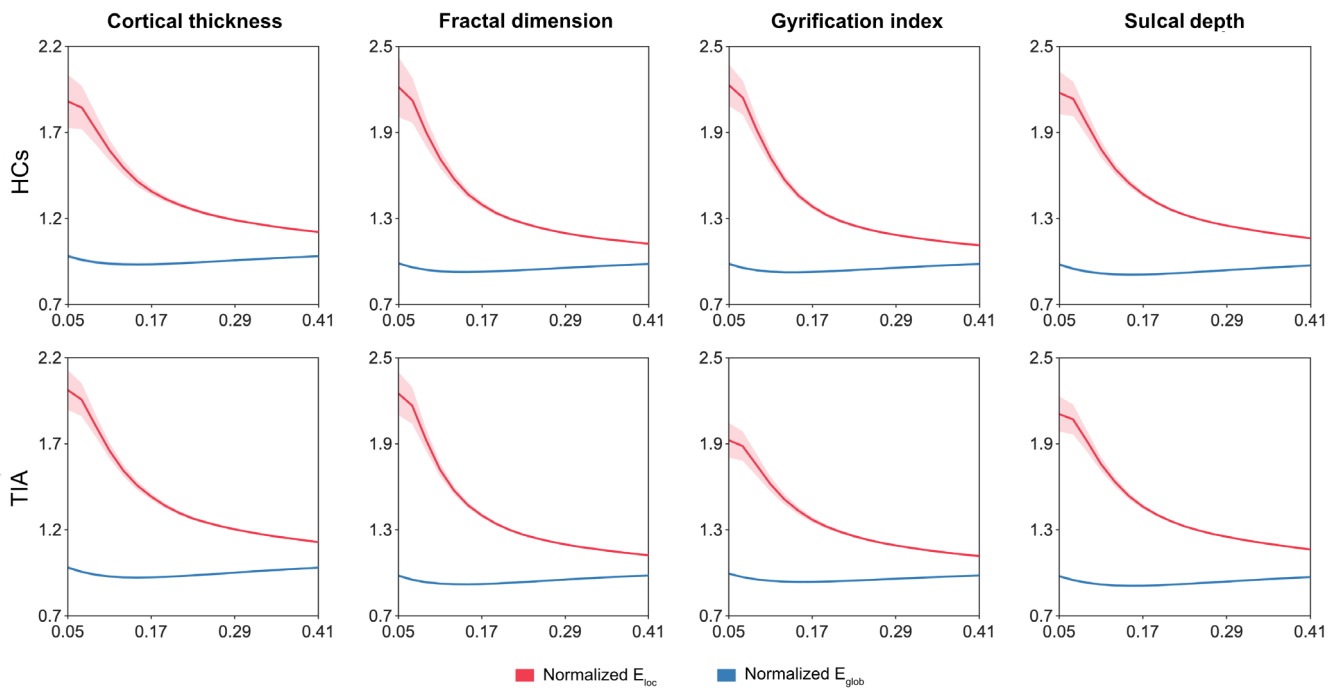

FIGURE 3 Small-world organization of whole-brain morphological networks as a function of sparsity thresholds. Highly efficient small-world organization was observed in all types of morphological brain networks of both groups as characterized by larger-than-1 normalized local efficiency and approximately-equal-to-1 normalized global efficiency. HCs, healthy controls; TIA, transient ischemic attack; E_{loc}, local efficiency; E_{glob}, global efficiency
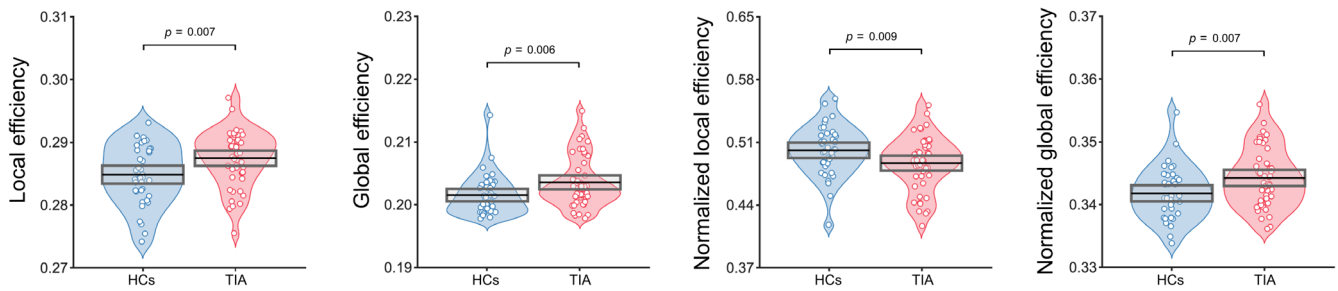
FIGURE 4 Altered network efficiency in transient ischemic attack (TIA). Compared with the healthy controls (HCs), the TIA patients exhibited significant increases in local efficiency, global efficiency and normalized global efficiency, and decreases in normalized local efficiency for gyrification index (GI)-based morphological brain networks

3.4.2 | Nodal centrality

We identified 41, 38, 38, and 34 hubs in the HCs, and 44, 40, 35, and 34 hubs in the TIA patients for the CT-, FD-, GI-, and SD-based morphological brain networks, respectively (Figure 5). The hubs overlapped to a great extent between the two groups with 31, 22, 24, and 30 hubs common to the HCs and TIA patients, resulting in dice coefficients of 0.729, 0.564, 0.658, and 0.882 for the CT-, FD-, GI-, and SD-based networks, respectively. According to the functional connectivity networks proposed by Yeo et al. (2011), the distribution of nodes in these networks was consistent between two groups for the CT-based ($r = .982$, $p = .001$), GI-based ($r = .807$, $p = .020$), and SD-based ($r = .990$, $p = .005$) networks except for FD-based networks ($r = .690$, $p = .063$) (Figure 6). In addition, we noted that the hubs were involved in more sulci than gyri for the CT-, FD-, and SD-based networks in both the HCs (CT: 27 vs. 11; FD: 23 vs. 10; SD: 22 vs. 12) and TIA patients (CT: 30 vs. 9; FD: 23 vs. 14; SD: 24 vs. 10), while the numbers of sulci and gyri in hubs were similar for GI-based network (HCs: 18 vs. 17; TIA: 18 vs. 16) (Figure 5).

Quantitative comparisons revealed that relative to the HCs, the TIA patients showed significant alterations in nodal centrality only for the FD-based morphological brain networks ($p < .05$, Bonferroni corrected), as characterized by decreased nodal degree ($p = .0002$, Cohen's $d = 0.918$), efficiency ($p = .0002$, Cohen's $d = 0.923$), eigenvector ($p = .0001$, Cohen's $d = 0.932$), and page-rank ($p = .0001$, Cohen's $d = 0.882$) in the right middle frontal gyrus (Figure 7). No regions exhibited significant between-group differences in any nodal centrality measures for the CT-, GI-, or SD-based morphological brain networks ($p > .05$, Bonferroni corrected).

Of note, the reported results did not survive when the multiple comparison correction was performed across all tests (2,932 = 4 morphological indices × 4 global measures + 4 morphological indices × 5 nodal centrality measures × 148 nodes) ($p > .05$, Bonferroni corrected).

3.5 | Brain-clinical relationships in the TIA patients

For the regions, edges and network measures showing TIA-related morphological alterations, no significant correlations were found with any clinical variable in the patients ($p > .05$, Bonferroni corrected; Supplementary Table 1).

3.6 | Sensitivity and specificity of morphological metrics in classification of TIA

For the regions, edges and network measures showing TIA-related morphological alterations, the mean strength of decreased morphological connectivity exhibited the highest accuracy for distinguishing the TIA patients from HCs. Specifically, 44 out of the 50 patients with TIA and 34 out of the 40 HCs were classified correctly for the mean connectivity strength of the FD-based component (accuracy = 86.7%, sensitivity = 88.0%, specificity = 87.5%, AUC = 0.939, $p < .001$), and 47 out of the 50 patients and 34 out of the 40 HCs were classified correctly for the mean connectivity strength of the GI-based component (accuracy = 90.0%, sensitivity = 94.0%, specificity = 85.0%, AUC = 0.934, $p < .001$) (Figure 8). All the other measures exhibited relatively poor discriminant performance (AUC <0.8).

For the SVM-based analyses, poor discriminant performance was found regardless of the features used (accuracy <0.7; Supplementary Table 2).

3.7 | Effect of follow-up ischemic attacks in the TIA patients

For the regions, edges and network measures showing TIA-related morphological alterations, no significant differences were found between the patients suffering from ischemic attacks in 1 year after the MR scanning and those without follow-up ischemic attacks ($p > .05$, Bonferroni corrected; Supplementary Table 3).

3.8 | Results of validation analyses

For the regions, edges and network measures showing TIA-related morphological alterations, no significant differences were found
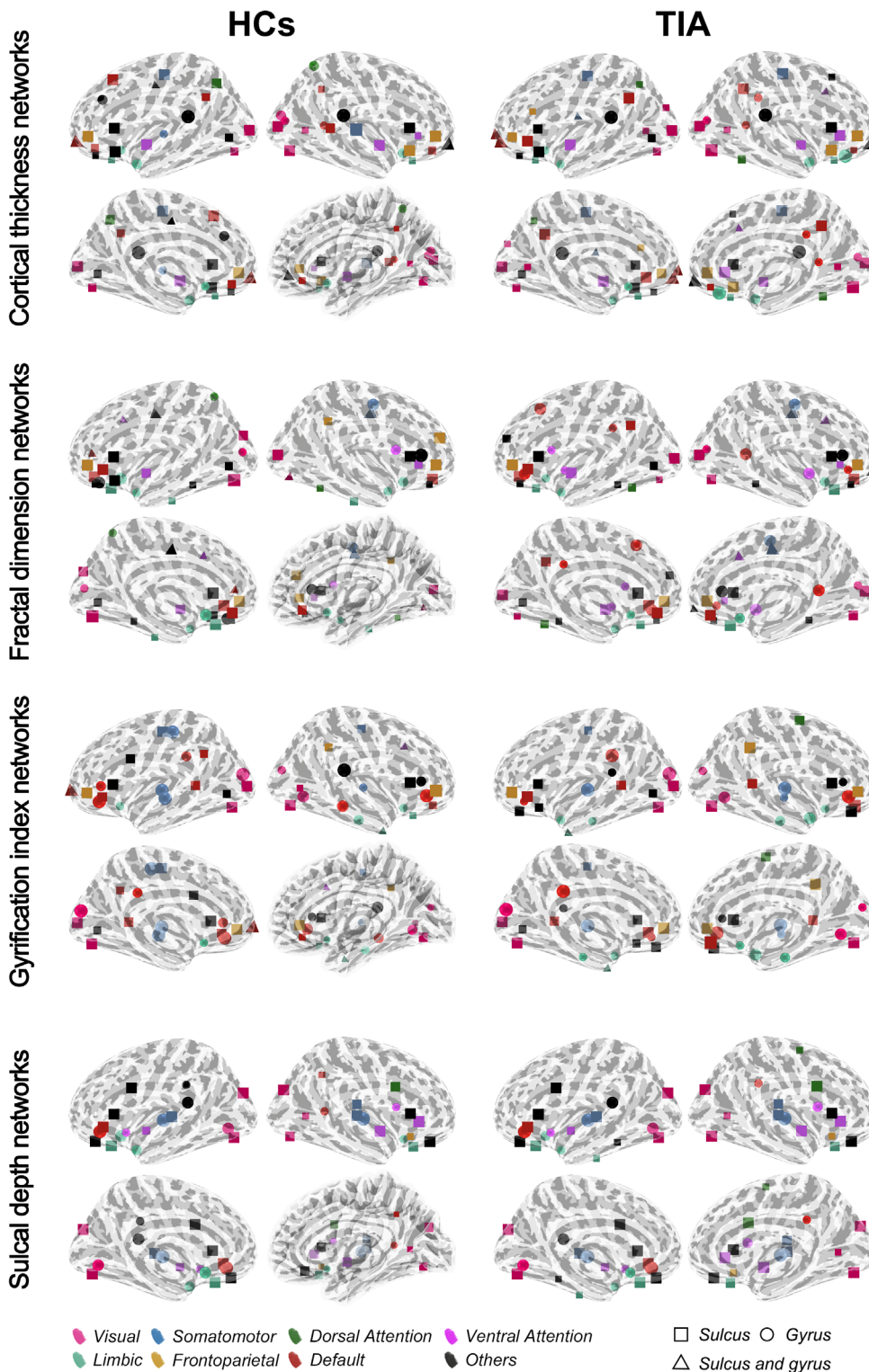
FIGURE 5 Hubs in whole-brain morphological networks. Nodal size indicates the times a node was identified as a hub among five nodal centrality measures. HCs, healthy controls; TIA, transient ischemic attack

between the patients with more than an ischemic attack and the patients who suffered first-time ischemic attack ($p > .05$, Bonferroni corrected), no significant correlations were found with the symptom durations of the last TIA attack for the patients ($p > .05$, Bonferroni corrected), and largely comparable patterns were observed after excluding the six patients with brain lesions (Supplementary Tables 4–6).

4 | DISCUSSION

In the current study, we employed four surface mesh-based indices to investigate morphological alterations in patients with TIA at three levels. We found widespread morphological alterations in TIA and the alterations were dependent on the choices of morphological index and analytical level. These findings provide evidence for the
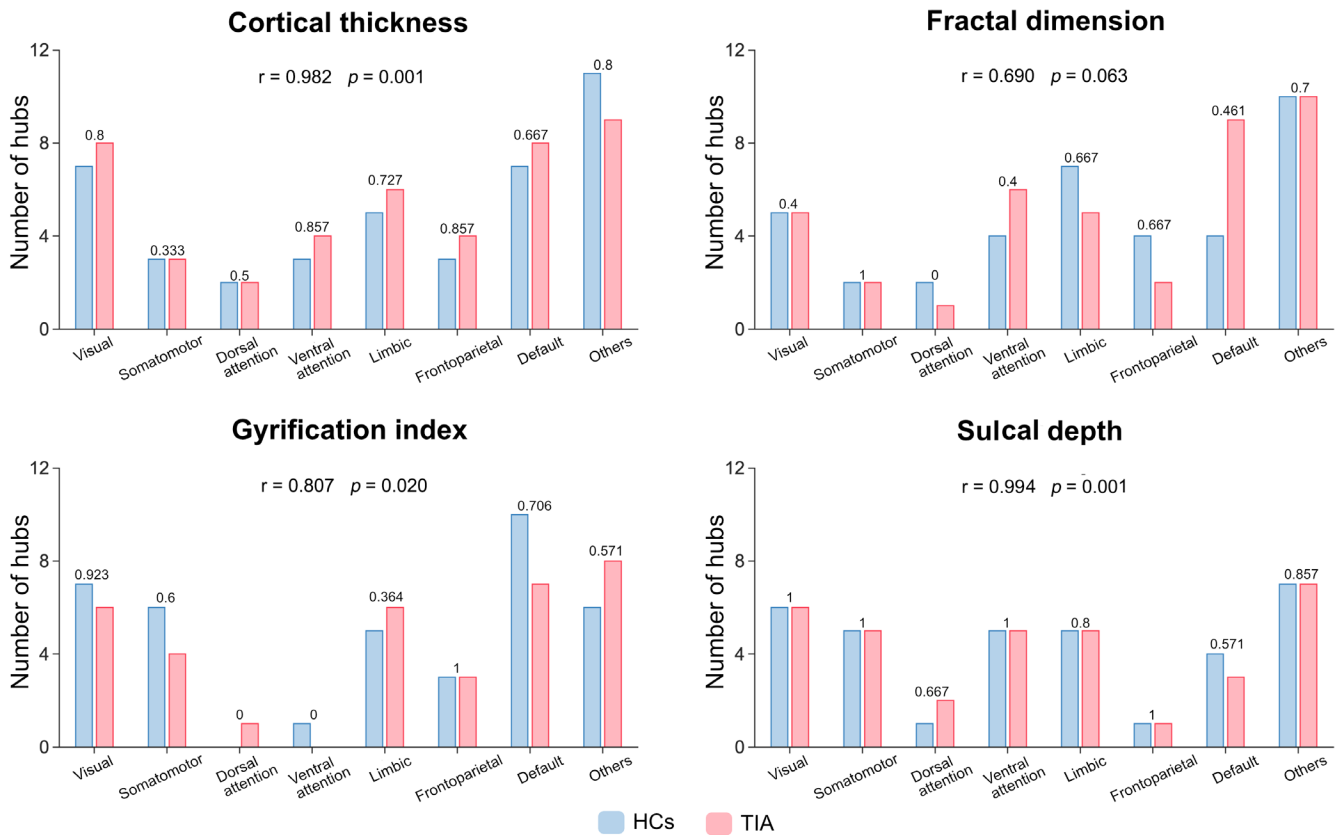
FIGURE 6 Hub distribution in the context of functional subnetworks. Similar hub distributions were observed between the transient ischemic attack (TIA) patients and healthy controls (HCs) at the functional subnetwork level for cortical thickness (CT)-, gyrification index (GI)-, and sulcal depth (SD)-based but not fractal dimension (FD)-based morphological brain networks. Numbers above the bars are dice coefficients of hubs between the two groups

emergence of profound morphological alterations in TIA, and highlight the complementary nature of different morphological indices and analytical levels in completely characterizing cortical morphology in health and disease.

First, for local morphological topography, reduced CT was observed in the patients in the left anterior transverse temporal gyrus, left posterior ramus of the lateral sulcus and right vertical ramus of the anterior segment of the lateral sulcus. The temporal transverse gyrus, known also as the Heschl gyrus, is situated on the superior temporal gyrus at the upper surface of the temporal lobe and buried deep in the lateral fissure of Sylvius (Simon et al., 2013). Previous studies have indicated that the left anterior transverse temporal gyrus is associated with auditory perception, music processing, language-related cognition, speech execution and motor learning (Koelsch, 2005; Sugata et al., 2020; Wensing et al., 2017). As a part of the inferior parietal lobule, the left posterior ramus of the lateral sulcus is involved in motor execution and pain perception (Du, Xiao, & Zuo, 2018; Hetu et al., 2013; Yang, 2015). The right vertical ramus of the anterior segment of the lateral sulcus, which extends dorsally into the inferior frontal gyrus, is related to time and pain perception (Meyer, Williams, & Eisenberger, 2015; Teghil et al., 2019). Given that patients with TIA exhibit persistent cognitive impairments, including motor execution, auditory perception and speech execution, we speculate

that the decreased CT in these three regions may, at least partially, contribute to these cognitive deficits in TIA.

Second, for interregional morphological connectivity, decreases were observed in the patients for FD- and GI-based morphological brain networks. Moreover, the decreases were mainly involved in interhemispheric connections. Impaired interhemispheric connectivity has been previously reported in patients with stroke and TIA for functional brain networks (Lv, Han, et al., 2019; Wang et al., 2010). Thus, our findings of disrupted interhemispheric morphological connectivity may be structural substrate of the impaired interhemispheric functional connectivity in the disease. Interestingly, consistent with our previous study (Lv, Han, et al., 2019), the decreased connectivity exhibited excellent performance for differentiating the TIA patients from HCs. These findings together indicate that impaired interhemispheric connectivity may serve as a reliable biomarker for diagnosis of ischemic attacks.

Finally, for whole-brain network organization, we found efficient small-world organization for all types of morphological brain networks in both TIA patients and HCs. These results suggest the preservation of an optimal organization of the patients' brains to support efficient information transfer of both modular and distributed processing. Nevertheless, quantitative comparisons revealed increased local and global efficiency for GI-based morphological brain networks in the
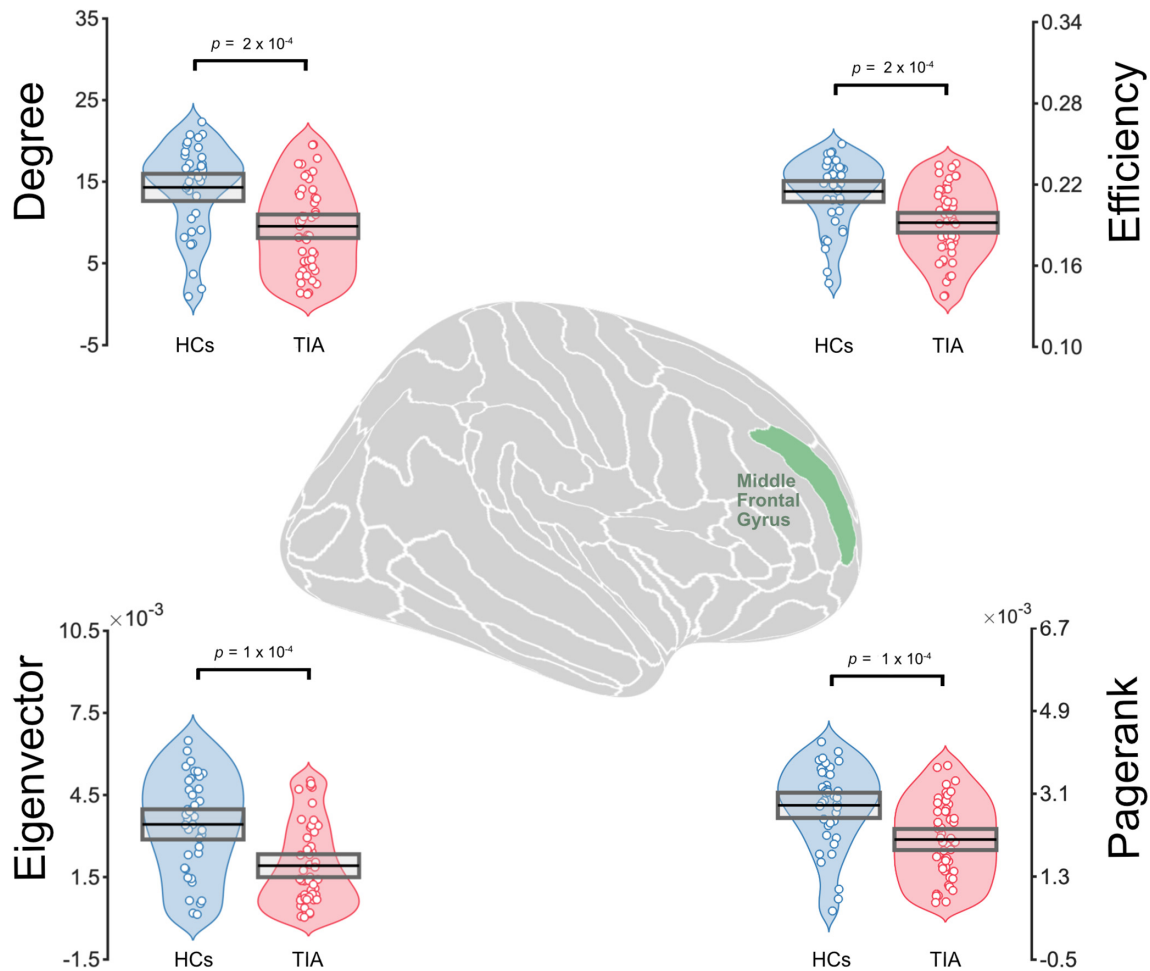
FIGURE 7 Decreased nodal centrality in transient ischemic attack (TIA). Compared with the healthy controls (HCs), the TIA patients showed decreased nodal degree, efficiency, eigenvector, and page-rank in the right middle frontal gyrus for fractal dimension (FD)-based morphological brain networks ($p < .05$, Bonferroni corrected)

patients with TIA. Local efficiency is predominantly associated with short-range connections between nearby regions and reflects modular information processing of the brain, whereas the global efficiency is mainly associated with long-range connections and reflects integrative information processing between and across remote regions of the brain. Thus, the observed increases suggest impaired functional segregation and integration in TIA. When normalized by random networks, global efficiency remained increased, while local efficiency was decreased in the patients. These findings suggest a shift toward random configurations in the TIA patients' brains that favor lower local coordination compared to the small-world organization and thus may lead to less modularized and more distributed processing information processing. It should be noted that the global network alterations were contrary to our previous functional network study, which observed decreased local, global and normalized global efficiency in TIA (Lv, Han, et al., 2019). The disagreement may reflect distinct neural mechanisms that govern morphological and functional brain network alterations in TIA. This speculation sounds plausible given poor correspondence between morphological and functional brain networks (Reid et al., 2016). In the future, it is important to examine

common and specific network alterations in TIA by combining multi-modal MRI techniques.

For regional organization of whole-brain morphological networks, some frontal and occipital regions, such as inferior frontal gyrus and anterior occipital sulcus, were consistently identified as hubs as characterized by their central placement in the morphological brain networks in terms of different centrality measures. The regions are consistent with previous findings from other modalities or approaches of brain networks (van den Heuvel & Sporns, 2013). Moreover, the hubs overlapped to a great extent between the TIA patients and HCs regardless of the type of morphological brain networks. These findings indicate the integrity of hub regions in contributing to overall network function in TIA. Interestingly, we noted that the hubs involved more sulci than gyri for the CT-, FD-, and SD-based morphological brain networks in both groups, suggesting a greater role of sulci than gyri in coordinating the networks. Analogous to largely intact hubs in TIA, quantitative centrality comparisons of all nodes revealed only one region (i.e., the right middle frontal gyrus) that showed decreases in the patients for FD-based morphological brain networks. The decrease may be implicated in cognitive impairments in TIA given the
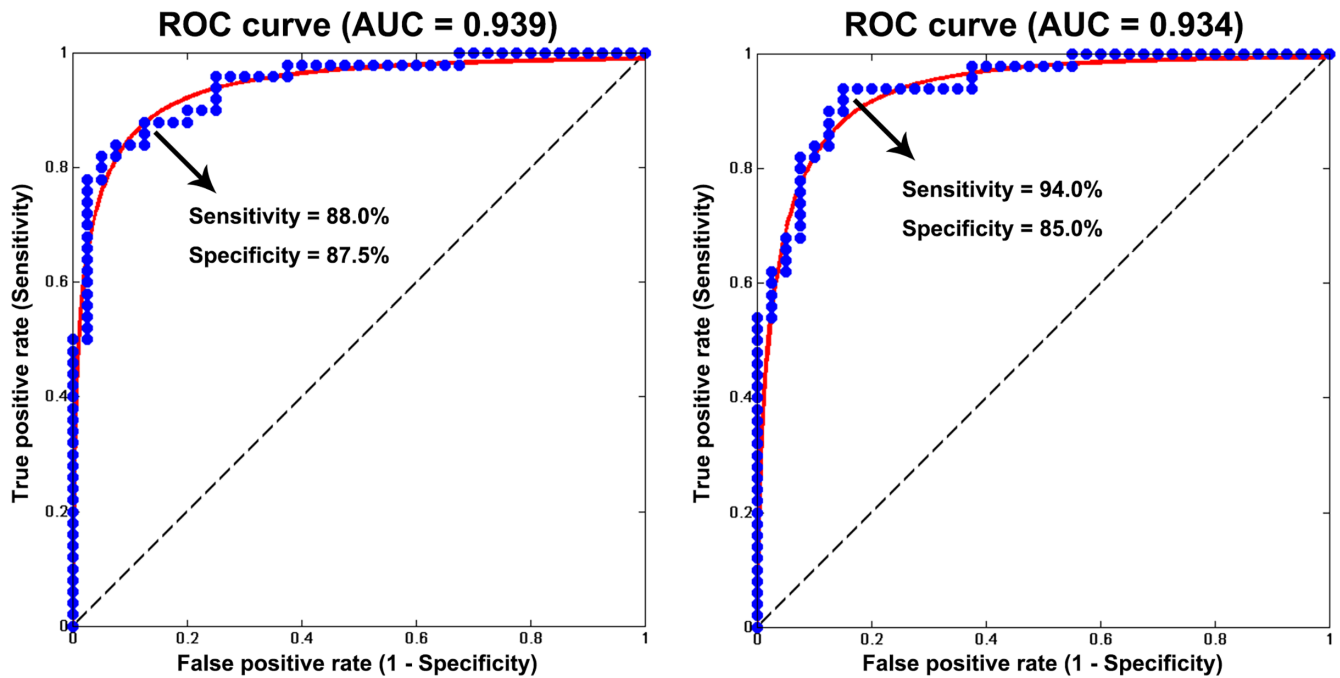
FIGURE 8 Transient ischemic attack (TIA)-control classification. The mean strength of impaired fractal dimension (FD)-based (a) and gyrification index (GI)-based (b) morphological connectivity in transient ischemic attack (TIA) distinguished the patients from healthy controls (HCs) with high sensitivities and specificities. AUC, area under curve; ROC, receiver operating characteristic

involvement of the right middle frontal gyrus in attention and working memory (Japee, Holiday, Satyshur, Mukai, & Ungerleider, 2015).

It should be emphasized that the TIA-related morphological alterations seem to depend on the choices of morphological index and analytical level based on which between-group comparisons were conducted. Specifically, TIA-related regional morphological alterations appeared to occur only in CT, while impaired interregional connectivity and disrupted whole-brain topology appeared to emerge only in folding-based (i.e., FD and GI) morphological indices. These findings suggest different mechanisms that drive the TIA-related morphological alterations in CT and cortical folding. CT, which captures the laminar structure of the cortex, reflects the size, density and arrangement of cells (neurons, neuroglia, and nerve fibers) in the cerebral cortex (Narr et al., 2005), while the folding-based indices represent the complexity of the cerebral surface (Luders et al., 2006; Van Essen et al., 2006; Yotter, Nenadic, Ziegler, Thompson, & Gaser, 2011). The cortical folding may result from different neurodevelopmental rates of expansion of superficial and deep cortical layers, which vastly increases cortical surface area relative to the cranium. A previous study has shown that cortical folding (indexed by local GI) and surface area were positively related, both of which correlated negatively with CT (Hogstrom et al., 2013), indicating increasing local gyrification and arealization with decreasing CT. In addition to the different cellular mechanisms, distinct genetic origins (Panizzon et al., 2009; Strike et al., 2019; Winkler et al., 2010) and differential developmental/aging trajectories (Hogstrom et al., 2013; Raznahan et al., 2011; Wierenga et al., 2014) have been frequently reported between cortical folding/surface area and CT. These distinct characteristics in cellular

mechanisms, genetic origins and developmental/aging trajectories between CT and cortical folding may result in their different susceptibilities to analytical levels in revealing TIA-related alterations. Of note, evidence from previous computational modeling studies has shown that increased cortical folding might be more efficient means to facilitate brain connectivity and functional development than increasing the thickness of the cortex (Murre & Sturdy, 1995; Ruppin, Schwartz, & Yeshurun, 1993). It is thus an interesting topic in the future to explore whether TIA-related morphological alterations in cortical folding can account for cognitive impairments of the patients to a greater extent than those in CT.

This study has several limitations. First, this is a cross-sectional study. It is important for future studies to trace longitudinal morphological changes as TIA progresses. Second, this study lacked cognitive data for the patients. It would be interesting to investigate cognitive relevance of the observed TIA-related morphological alterations in the future. Third, given that TIA is an important risk factor for stroke, it is interesting to explore trajectories of morphological alterations along the continuum from TIA to stroke. Fourth, we did not collect the information of TIA attack times for the patients with TIA history, which may confound our findings. It is interesting for future studies to examine the relationships between TIA attack times and morphological brain architecture in the patients. Fifth, only four surface-based morphological indices that were calculated with the CAT12 toolbox were used in this study. A more complete mapping of TIA-related morphological alterations can benefit from analyzing other morphological indices that are computationally available in different toolboxes, such as surface area and surface normal. Finally, our findings

did not survive multiple comparison correction across all tests, and thus may be false positive results. Presumably, this may be due to small sample size of this study and/or large variation in the TIA attack times of the patients. These two factors may also explain why we did not observe significant correlations between TIA-related morphological alterations and clinical variables of the patients and poor discriminant performance between the patients and controls by SVM (Cui & Gong, 2018). Future studies are required to examine the reproducibility of our findings by recruiting more and clinically homogeneous patients.

5 | CONCLUSIONS

This study demonstrates that the emergence of morphological index-dependent and analytical level-specific morphological alterations in TIA, which provide novel insights into mechanisms underlying TIA and may serve as potential biomarkers to help early diagnosis of the disease. Meanwhile, our findings highlight the necessity of multiparametric and multilevel approaches for a complete mapping of cerebral morphology in health and disease.

CONFLICT OF INTEREST
The authors declare no conflict of interests.

DATA AVAILABILITY STATEMENT
According to the privacy protection policy of the Center for Cognition and Brain Disorders, Hangzhou Normal University, all data that support the findings of this study is not available in open access. However, researchers who are interested in accessing data could contact the corresponding author, who will help contact the committee of the center for data requisition.

ORCID
Yating Lv https://orcid.org/0000-0002-5547-3361
Ningkai Wang https://orcid.org/0000-0002-2363-9021

REFERENCES
Achard, S., & Bullmore, E. (2007). Efficiency and cost of economical brain functional networks. *PLoS Computational Biology*, 3(2), e17. https://doi.org/10.1371/journal.pcbi.0030017

Achard, S., Salvador, R., Whitcher, B., Suckling, J., & Bullmore, E. (2006). A resilient, low-frequency, small-world human brain functional network with highly connected association cortical hubs. *The Journal of Neuroscience*, 26(1), 63–72. https://doi.org/10.1523/JNEUROSCI.3874-05.2006

Albers, G. W., Caplan, L. R., Easton, J. D., Fayad, P. B., Mohr, J. P., Saver, J. L., ... for the TIA Working Group. (2002). Transient ischemic attack—Proposal for a new definition. *The New England Journal of Medicine*, 347(21), 1713–1716. https://doi.org/10.1056/NEJMsb020987

Andrews, T. J., Halpern, S. D., & Purves, D. (1997). Correlated size variations in human visual cortex, lateral geniculate nucleus, and optic tract. *The Journal of Neuroscience*, 17(8), 2859–2868.

Bakker, F. C., Klijn, C. J., Jennekens-Schinkel, A., van der Tweel, I., Tulleken, C. A., & Kappelle, L. J. (2003). Cognitive impairment in patients with carotid artery occlusion and ipsilateral transient ischemic attacks. *Journal of Neurology*, 250(11), 1340–1347. https://doi.org/10.1007/s00415-003-0222-1

Bassett, D. S., Bullmore, E., Verchinski, B. A., Mattay, V. S., Weinberger, D. R., & Meyer-Lindenberg, A. (2008). Hierarchical organization of human cortical networks in health and schizophrenia. *The Journal of Neuroscience*, 28(37), 9239–9248. https://doi.org/10.1523/JNEUROSCI.1929-08.2008

Boldi, P., Santini, M., & Vigna, S. (2009). *PageRank: Functional dependencies* (p. 19). New York, NY: ACM Transactions on Information Systems. https://doi.org/10.1145/1629096.1629097

Bonacich, P. (1972). Factoring and weighting approaches to status scores and clique identification. *Journal of Mathematical Sociology*, 2(1), 113–120.

Chen, T., Kendrick, K. M., Wang, J., Wu, M., Li, K., Huang, X., ... Gong, Q. (2017). Anomalous single-subject based morphological cortical networks in drug-naive, first-episode major depressive disorder. *Human Brain Mapping*, 38(5), 2482–2494. https://doi.org/10.1002/hbm.23534

Cohen, J. (1969). *Statistical power analysis for the behavioral sciences*. New York, NY: Academic Press.

Cohen, J. (1987). *Statistical power analysis for the behavioral sciences*. Hillside, NJ: Lawrence Erlbaum Associates.

Cui, Z., & Gong, G. (2018). The effect of machine learning regression algorithms and sample size on individualized behavioral prediction with functional connectivity features. *NeuroImage*, 178, 622–637. https://doi.org/10.1016/j.neuroimage.2018.06.001

Dahnke, R., Yotter, R. A., & Gaser, C. (2013). Cortical thickness and central surface estimation. *NeuroImage*, 65, 336–348. https://doi.org/10.1016/j.neuroimage.2012.09.050

Destrieux, C., Fischl, B., Dale, A., & Halgren, E. (2010). Automatic parcellation of human cortical gyri and sulci using standard anatomical nomenclature. *NeuroImage*, 53(1), 1–15. https://doi.org/10.1016/j.neuroimage.2010.06.010

Du, J. G., Xiao, H., & Zuo, Y. X. (2018). Amplitude of low frequency fluctuation (ALFF) study of the spontaneous brain activities of patients with phantom limb pain. *European Review for Medical and Pharmacological Sciences*, 22(21), 7164–7171. https://doi.org/10.26355/eurrev_201811_16248

Easton, J. D., Saver, J. L., Albers, G. W., Alberts, M. J., Chaturvedi, S., Feldmann, E., ... Interdisciplinary Council on Peripheral Vascular Disease. (2009). Definition and evaluation of transient ischemic attack: A scientific statement for healthcare professionals from the American Heart Association/American Stroke Association Stroke Council; Council on Cardiovascular Surgery and Anesthesia; Council on Cardiovascular Radiology and Intervention; Council on Cardiovascular Nursing; and the Interdisciplinary Council on Peripheral Vascular Disease. The American Academy of Neurology affirms the value of this statement as an educational tool for neurologists. *Stroke*, 40(6), 2276–2293. https://doi.org/10.1161/STROKEAHA.108.192218

Freeman, L. (1977). A set of measures of centrality based on betweenness. *Sociometry*, 40(1), 35–41.

Giles, M. F., & Rothwell, P. M. (2007). Risk of stroke early after transient ischaemic attack: A systematic review and meta-analysis. *Lancet Neurology*, 6(12), 1063–1072. https://doi.org/10.1016/S1474-4422(07)70274-0

Guo, J., Chen, N., Li, R., Wu, Q., Chen, H., Gong, Q., & He, L. (2014). Regional homogeneity abnormalities in patients with transient ischaemic attack: A resting-state fMRI study. *Clinical Neurophysiology*, *125*(3), 520–525. https://doi.org/10.1016/j.clinph.2013.08.010

He, Y., Chen, Z. J., & Evans, A. C. (2007). Small-world anatomical networks in the human brain revealed by cortical thickness from MRI. *Cerebral Cortex*, *17*(10), 2407–2419. https://doi.org/10.1093/cercor/bhl149

Hetu, S., Gregoire, M., Saimpont, A., Coll, M. P., Eugene, F., Michon, P. E., & Jackson, P. L. (2013). The neural network of motor imagery: An ALE meta-analysis. *Neuroscience and Biobehavioral Reviews*, *37*(5), 930–949. https://doi.org/10.1016/j.neubiorev.2013.03.017

Hogstrom, L. J., Westlye, L. T., Walhovd, K. B., & Fjell, A. M. (2013). The structure of the cerebral cortex across adult life: Age-related patterns of surface area, thickness, and gyrification. *Cerebral Cortex*, *23*(11), 2521–2530. https://doi.org/10.1093/cercor/bhs231

Hutton, C., Draganski, B., Ashburner, J., & Weiskopf, N. (2009). A comparison between voxel-based cortical thickness and voxel-based morphometry in normal aging. *NeuroImage*, *48*(2), 371–380. https://doi.org/10.1016/j.neuroimage.2009.06.043

Japee, S., Holiday, K., Satyshur, M. D., Mukai, I., & Ungerleider, L. G. (2015). A role of right middle frontal gyrus in reorienting of attention: A case study. *Frontiers in Systems Neuroscience*, *9*, 23. https://doi.org/10.3389/fnsys.2015.00023

Johnston, S. C., Rothwell, P. M., Nguyen-Huynh, M. N., Giles, M. F., Elkins, J. S., Bernstein, A. L., & Sidney, S. (2007). Validation and refinement of scores to predict very early stroke risk after transient ischaemic attack. *Lancet*, *369*(9558), 283–292. https://doi.org/10.1016/S0140-6736(07)60150-0

Koelsch, S. (2005). Neural substrates of processing syntax and semantics in music. *Current Opinion in Neurobiology*, *15*(2), 207–212. https://doi.org/10.1016/j.conb.2005.03.005

Kong, X. Z., Liu, Z., Huang, L., Wang, X., Yang, Z., Zhou, G., ... Liu, J. (2015). Mapping individual brain networks using statistical similarity in regional morphology from MRI. *PLoS One*, *10*(11), e0141840. https://doi.org/10.1371/journal.pone.0141840

Latora, V., & Marchiori, M. (2001). Efficient behavior of small-world networks. *Physical Review Letters*, *87*(19), 198701. https://doi.org/10.1103/PhysRevLett.87.198701

Lerch, J. P., Worsley, K., Shaw, W. P., Greenstein, D. K., Lenroot, R. K., Giedd, J., & Evans, A. C. (2006). Mapping anatomical correlations across cerebral cortex (MACACC) using cortical thickness from MRI. *NeuroImage*, *31*(3), 993–1003. https://doi.org/10.1016/j.neuroimage.2006.01.042

Li, J., & Kong, X. Z. (2017). Morphological connectivity correlates with trait impulsivity in healthy adults. *PeerJ*, *5*, e3533. https://doi.org/10.7717/peerj.3533

Li, R., Guo, J., Ma, X., Wang, S., Zhang, J., He, L., ... Chen, H. (2015). Alterations in the gray matter volume in transient ischemic attack: A voxel-based morphometry study. *Neurological Research*, *37*(1), 43–49. https://doi.org/10.1179/1743132814Y.0000000406

Li, R., Wang, S., Zhu, L., Guo, J., Zeng, L., Gong, Q., ... Chen, H. (2013). Aberrant functional connectivity of resting state networks in transient ischemic attack. *PLoS One*, *8*(8), e71009. https://doi.org/10.1371/journal.pone.0071009

Luders, E., Thompson, P. M., Narr, K. L., Toga, A. W., Jancke, L., & Gaser, C. (2006). A curvature-based approach to estimate local gyrification on the cortical surface. *NeuroImage*, *29*(4), 1224–1230. https://doi.org/10.1016/j.neuroimage.2005.08.049

Lv, Y., Han, X., Song, Y., Han, Y., Zhou, C., Zhou, D., ... Wang, J. (2019). Toward neuroimaging-based network biomarkers for transient ischemic attack. *Human Brain Mapping*, *40*(11), 3347–3361. https://doi.org/10.1002/hbm.24602

Lv, Y., Li, L., Song, Y., Han, Y., Zhou, C., Zhou, D., ... Han, X. (2019). The local brain abnormalities in patients with transient ischemic attack: A

resting-state fMRI study. *Frontiers in Neuroscience*, *13*, 24. https://doi.org/10.3389/fnins.2019.00024

Maslov, S., & Sneppen, K. (2002). Specificity and stability in topology of protein networks. *Science*, *296*(5569), 910–913. https://doi.org/10.1126/science.1065103

Meyer, M. L., Williams, K. D., & Eisenberger, N. I. (2015). Why social pain can live on: Different neural mechanisms are associated with reliving social and physical pain. *PLoS One*, *10*(6), e0128294. https://doi.org/10.1371/journal.pone.0128294

Milo, R., Shen-Orr, S., Itzkovitz, S., Kashtan, N., Chklovskii, D., & Alon, U. (2002). Network motifs: Simple building blocks of complex networks. *Science*, *298*(5594), 824–827. https://doi.org/10.1126/science.298.5594.824

Murre, J. M., & Sturdy, D. P. (1995). The connectivity of the brain: Multi-level quantitative analysis. *Biological Cybernetics*, *73*(6), 529–545. https://doi.org/10.1007/BF00199545

Narr, K. L., Bilder, R. M., Toga, A. W., Woods, R. P., Rex, D. E., Szeszko, P. R., ... Thompson, P. M. (2005). Mapping cortical thickness and gray matter concentration in first episode schizophrenia. *Cerebral Cortex*, *15*(6), 708–719. https://doi.org/10.1093/cercor/bhh172

Panizzon, M. S., Fennema-Notestine, C., Eyler, L. T., Jernigan, T. L., Prom-Wormley, E., Neale, M., ... Kremen, W. S. (2009). Distinct genetic influences on cortical surface area and cortical thickness. *Cerebral Cortex*, *19*(11), 2728–2735. https://doi.org/10.1093/cercor/bhp026

Raznahan, A., Shaw, P., Lalonde, F., Stockman, M., Wallace, G. L., Greenstein, D., ... Giedd, J. N. (2011). How does your cortex grow? *Journal of Neuroscience*, *31*(19), 7174–7177.

Reid, A. T., Lewis, J., Bezgin, G., Khundrakpam, B., Eickhoff, S. B., McIntosh, A. R., ... Evans, A. C. (2016). A cross-modal, cross-species comparison of connectivity measures in the primate brain. *NeuroImage*, *125*, 311–331. https://doi.org/10.1016/j.neuroimage.2015.10.057

Righart, R., Schmidt, P., Dahnke, R., Biberacher, V., Beer, A., Buck, D., ... Muhlau, M. (2017). Volume versus surface-based cortical thickness measurements: A comparative study with healthy controls and multiple sclerosis patients. *PLoS One*, *12*(7), e0179590. https://doi.org/10.1371/journal.pone.0179590

Ruppin, E., Schwartz, E. L., & Yeshurun, Y. (1993). Examining the volume efficiency of the cortical architecture in a multi-processor network model. *Biological Cybernetics*, *70*(1), 89–94. https://doi.org/10.1007/BF00202570

Sachdev, P. S., Brodaty, H., Valenzuela, M. J., Lorentz, L., Looi, J. C., Wen, W., & Zagami, A. S. (2004). The neuropsychological profile of vascular cognitive impairment in stroke and TIA patients. *Neurology*, *62*(6), 912–919. https://doi.org/10.1212/01.wnl.0000115108.65264.4b

Schultz-Larsen, K., Lomholt, R. K., & Kreiner, S. (2007). Mini-mental status examination: A short form of MMSE was as accurate as the original MMSE in predicting dementia. *Journal of Clinical Epidemiology*, *60*(3), 260–267. https://doi.org/10.1016/j.jclinepi.2006.06.008

Seidlitz, J., Vasa, F., Shinn, M., Romero-Garcia, R., Whitaker, K. J., Vertes, P. E., ... Bullmore, E. T. (2018). Morphometric similarity networks detect microscale cortical organization and predict inter-individual cognitive variation. *Neuron*, *97*(1), 231–247 e237. https://doi.org/10.1016/j.neuron.2017.11.039

Seiger, R., Ganger, S., Kranz, G. S., Hahn, A., & Lanzenberger, R. (2018). Cortical thickness estimations of FreeSurfer and the CAT12 toolbox in patients with Alzheimer's disease and healthy controls. *Journal of Neuroimaging*, *28*(5), 515–523. https://doi.org/10.1111/jon.12521

Simon, E., Perrot, X., Linne, M., Afif, A., Becq, G., & Mertens, P. (2013). Morphometry and localization of the temporal transverse Heschl's gyrus in magnetic resonance imaging: A guide for cortical stimulation of chronic tinnitus. *Surgical and Radiologic Anatomy*, *35*(2), 115–124. https://doi.org/10.1007/s00276-012-1008-x

Strike, L. T., Hansell, N. K., Couvy-Duchesne, B., Thompson, P. M., de Zubicaray, G. I., McMahon, K. L., & Wright, M. J. (2019). Genetic

complexity of cortical structure: Differences in genetic and environmental factors influencing cortical surface area and thickness. *Cerebral Cortex*, 29(3), 952–962. https://doi.org/10.1093/cercor/bhy002

Su, W., Guo, J., Zhang, Y., Zhou, J., Chen, N., Zhou, M., ... He, L. (2018). A longitudinal functional magnetic resonance imaging study of working memory in patients following a transient ischemic attack: A preliminary study. *Neuroscience Bulletin*, 34(6), 963–971. https://doi.org/10.1007/s12264-018-0270-2

Sugata, H., Yagi, K., Yazawa, S., Nagase, Y., Tsuruta, K., Ikeda, T., ... Kawakami, K. (2020). Role of beta-band resting-state functional connectivity as a predictor of motor learning ability. *NeuroImage*, 210, 116562. https://doi.org/10.1016/j.neuroimage.2020.116562

Teghil, A., Boccia, M., D'Antonio, F., di Vita, A., de Lena, C., & Guariglia, C. (2019). Neural substrates of internally-based and externally-cued timing: An activation likelihood estimation (ALE) meta-analysis of fMRI studies. *Neuroscience and Biobehavioral Reviews*, 96, 197–209. https://doi.org/10.1016/j.neubiorev.2018.10.003

Tian, L., Wang, J., Yan, C., & He, Y. (2011). Hemisphere- and gender-related differences in small-world brain networks: A resting-state functional MRI study. *NeuroImage*, 54(1), 191–202. https://doi.org/10.1016/j.neuroimage.2010.07.066

Tijms, B. M., Series, P., Willshaw, D. J., & Lawrie, S. M. (2012). Similarity-based extraction of individual networks from gray matter MRI scans. *Cerebral Cortex*, 22(7), 1530–1541. https://doi.org/10.1093/cercor/bhr221

van den Heuvel, M. P., & Sporns, O. (2013). Network hubs in the human brain. *Trends in Cognitive Sciences*, 17(12), 683–696. https://doi.org/10.1016/j.tics.2013.09.012

van Essen, D. C., Dierker, D., Snyder, A. Z., Raichle, M. E., Reiss, A. L., & Korenberg, J. (2006). Symmetry of cortical folding abnormalities in Williams syndrome revealed by surface-based analyses. *The Journal of Neuroscience*, 26(20), 5470–5483. https://doi.org/10.1523/JNEUROSCI.4154-05.2006

Voets, N. L., Hough, M. G., Douaud, G., Matthews, P. M., James, A., Winmill, L., ... Smith, S. (2008). Evidence for abnormalities of cortical development in adolescent-onset schizophrenia. *NeuroImage*, 43(4), 665–675. https://doi.org/10.1016/j.neuroimage.2008.08.013

Wang, H., Jin, X., Zhang, Y., & Wang, J. (2016). Single-subject morphological brain networks: Connectivity mapping, topological characterization and test-retest reliability. *Brain and Behavior: A Cognitive Neuroscience Perspective*, 6(4), e00448. https://doi.org/10.1002/brb3.448

Wang, J., Wang, L., Zang, Y., Yang, H., Tang, H., Gong, Q., ... He, Y. (2009). Parcellation-dependent small-world brain functional networks: A resting-state fMRI study. *Human Brain Mapping*, 30(5), 1511–1523. https://doi.org/10.1002/hbm.20623

Wang, L., Yu, C., Chen, H., Qin, W., He, Y., Fan, F., ... Zhu, C. (2010). Dynamic functional reorganization of the motor execution network after stroke. *Brain*, 133(Pt 4), 1224–1238. https://doi.org/10.1093/brain/awq043

Watts, D. J., & Strogatz, S. H. (1998). Collective dynamics of 'small-world' networks. *Nature*, 393(6684), 440–442. https://doi.org/10.1038/30918

Wensing, T., Cieslik, E. C., Muller, V. I., Hoffstaedter, F., Eickhoff, S. B., & Nickl-Jockschat, T. (2017). Neural correlates of formal thought disorder: An activation likelihood estimation meta-analysis. *Human Brain Mapping*, 38(10), 4946–4965. https://doi.org/10.1002/hbm.23706

Wierenga, L. M., Langen, M., Oranje, B., & Durston, S. (2014). Unique developmental trajectories of cortical thickness and surface area. *NeuroImage*, 87, 120–126. https://doi.org/10.1016/j.neuroimage.2013.11.010

Winkler, A. M., Kochunov, P., Blangero, J., Almasy, L., Zilles, K., Fox, P. T., ... Glahn, D. C. (2010). Cortical thickness or grey matter volume? The importance of selecting the phenotype for imaging genetics studies. *NeuroImage*, 53(3), 1135–1146. https://doi.org/10.1016/j.neuroimage.2009.12.028

Yang, J. (2015). The influence of motor expertise on the brain activity of motor task performance: A meta-analysis of functional magnetic resonance imaging studies. *Cognitive, Affective, & Behavioral Neuroscience*, 15(2), 381–394. https://doi.org/10.3758/s13415-014-0329-0

Yeo, B. T., Krienen, F. M., Sepulcre, J., Sabuncu, M. R., Lashkari, D., Hollinshead, M., ... Buckner, R. L. (2011). The organization of the human cerebral cortex estimated by intrinsic functional connectivity. *Journal of Neurophysiology*, 106(3), 1125–1165. https://doi.org/10.1152/jn.00338.2011

Yotter, R. A., Dahnke, R., Thompson, P. M., & Gaser, C. (2011). Topological correction of brain surface meshes using spherical harmonics. *Human Brain Mapping*, 32(7), 1109–1124. https://doi.org/10.1002/hbm.21095

Yotter, R. A., Nenadic, I., Ziegler, G., Thompson, P. M., & Gaser, C. (2011). Local cortical surface complexity maps from spherical harmonic reconstructions. *NeuroImage*, 56(3), 961–973. https://doi.org/10.1016/j.neuroimage.2011.02.007

Yotter, R. A., Thompson, P. M., & Gaser, C. (2011). Algorithms to improve the reparameterization of spherical mappings of brain surface meshes. *Journal of Neuroimaging*, 21(2), e134–e147. https://doi.org/10.1111/j.1552-6569.2010.00484.x

Zalesky, A., Fornito, A., & Bullmore, E. T. (2010). Network-based statistic: Identifying differences in brain networks. *NeuroImage*, 53(4), 1197–1207. https://doi.org/10.1016/j.neuroimage.2010.06.041

Zhu, T., Li, L., Song, Y., Han, Y., Zhou, C., Zhou, D., ... Han, X. (2019). Altered functional connectivity within default mode network in patients with transient ischemic attack: A resting-state functional magnetic resonance imaging study. *Cerebrovascular Diseases*, 48(1–2), 61–69. https://doi.org/10.1159/000502884

SUPPORTING INFORMATION

Additional supporting information may be found online in the Supporting Information section at the end of this article.